https://doi.org/10.5194/egusphere-2023-736
Preprint. Discussion started: 21 June 2023
© Author(s) 2023. CC BY 4.0 License.

Surface dynamics and history of the calving cycle of the Astrolabe glacier (Antarctica) derived from optical imagery

Floriane Provost[1], Dimitri Zigone[1,2], Emmanuel Le Meur[3], Jean-Philippe Malet[1,2], and Clément Hibert[1,2]

[1]Ecole et Observatoire des Sciences de la Terre (EOST), CNRS UAR 830 - Université de Strasbourg, 5 rue Descartes, F-67084 Strasbourg, France
[2]Institut Terre et Environnement de Strasbourg (ITES), CNRS UMR 7063 - Université de Strasbourg, 5 rue Descartes, F-67084 Strasbourg, France
[3]Institut des Géosciences de l'Environnement (IGE), CNRS UMR 5001 - Université Grenoble Alpes, Grenoble

Correspondence: Floriane Provost - f.provost@unistra.fr

Abstract. The recent calving of the Astrolabe glacier (Terre Adélie, East Antarctica) in November 2021 presents an opportunity to better understand the processes leading to ice fracturing. Optical satellite imagery is used to retrieve the calving cycle of the glacier since 2000 by mapping the ice front location. A recent archive of high resolution optical images from Sentinel-2 is used to measure the ice motion and the ice strain rates for the period 2017-2021 in order to document fractures and rift evolution. These observations are compared with sea ice extent and concentration measurements. We found that a significant change in the sea ice melting periodicity at the vicinity of the Astrolabe glacier occurred in the last decade (2011-2021) with respect to previous observations (1979-2011). After 2011, the occurrence of consecutive years of high sea-ice concentration at the vicinity of the glacier seems to have favored the ice tongue spatial extension. This lead to an unprecedentedly observed extension of the ice tongue until November 2021. The analysis of strain rate time series revealed that the glacier dislocated suddenly in June 2021 in the middle of the winter before releasing an iceberg of around 20 km^2 in November 2021 at the onset of sea ice melting season. These observations suggest that although the presence of sea ice favors glacier extension, its buttressing effect may not be sufficient to prevent fracture opening.

1 Introduction

Defining the contribution of polar ice sheets to sea-level rise is a major concern for the society, and better understanding the processes and the factors controlling ice retreat is of paramount importance to simulate the ice-sheet response to global warming (Seroussi et al., 2020; Chambers et al., 2022). Coastal glaciers in polar regions differ from temperate mountain glaciers in terms of volumes, catchment sizes and thermal states associated to complex interactions with the ocean. The presence of floating tongues with marine terminus makes Antarctic glaciers more sensitive to the atmospheric and ocean dynamics (Gudmundsson et al., 2019; Olinger et al., 2019; Paolo et al., 2015; Pritchard et al., 2012; Christie et al., 2022). Most of the studies focused on the largest ice shelves and ice tongues of Western Antarctica (Walker et al., 2013; Liu et al., 2015; Massom et al., 2018; Rignot et al., 2019; Millan et al., 2022) and only a few studies have analyzed the behavior of smaller-size glaciers in East

https://doi.org/10.5194/egusphere-2023-736
Preprint. Discussion started: 21 June 2023
© Author(s) 2023. CC BY 4.0 License.

Antarctica (Miles et al., 2017). In this study, we document and analyze the evolution of the Astrolabe glacier's ice tongue and, in particular, its most recent calving event of November 2021.

The Astrolabe glacier is located in Terre Adélie, (140°E, 67°S) near the Dumont d'Urville French research station. The glacier outlet is ca. 8 km wide (Figure 1a), while the drainage basin stretches as much as 200 kilometers inland. It is characterized by a tongue of ice developing on the water, presenting a calving front of 6 km width (Figure 1a). Due to its proximity to the Dumont D'Urville research station, the glacier has been extensively instrumented over the last decades (Le Meur et al., 2014). However, the calving cycle of the glacier has never been documented and due to its small size, the Astrolabe glacier dynamic is not properly monitored with global value-added products such as the NASA MEaSUREs ITS_LIVE (doi:10.5067/6II6VW8LLWJ7). Recent observations show an unusual spatial extension of the ice tongue until November 2021 when a major calving event occurred (Figure 1b-d).

Ice-calving events result from rift opening and/or fracture propagation that usually pre-exist in the ice tongue for several months to years (Benn et al., 2007; Walker et al., 2013). The release of an iceberg during a calving event results from the extensive opening of these fractures that may be triggered by hydro-fracturing (Scambos et al., 2000), sub-glacial warm water intrusion and basal melting (Ritz et al., 2015; Rignot et al., 2019; Pritchard et al., 2012), ice heterogeneity (Borstad et al., 2017), bending of the ice due to flexural rebound after lake drainage (Banwell et al., 2013), thinning of the ice mélange within pre-existing rifts (Larour et al., 2021) or/and in the ice shelf itself (Liu et al., 2015; Larour et al., 2021), and decrease of the sea-ice buttressing (Massom et al., 2001, 2018; Wearing et al., 2020; Gomez-Fell et al., 2022). Conversely, changes in atmospheric and ocean dynamics favoring the presence of sea-ice may act as a protection and allow glacier extension (Gomez-Fell et al., 2022; Massom et al., 2018; Christie et al., 2022). These processes are still poorly understood, as they exhibit strong spatial and temporal variability, which are highly difficult to document with direct observations in Antarctica. Moreover, the effect of landfast sea-ice on the ice tongue remains unclear: is landfast sea ice buttressing the ice tongue and hence preventing fracture propagation or is landfast sea-ice buttressing insufficient to inhibit the fracture and only hold the ice tongue parts together until calving is possible?

In this study, we determine for the first time the ice tongue extension cycle of the Astrolabe glacier from high resolution optical satellite imagery (Landsat, Sentinel-2 and ASTER) over the period 2000-2021. We also show the added-value of optical satellite images to monitor fractures propagation using ice velocity and strain rate calculated with optical image correlation. We compare these data to the sea-ice extent around the Astrolabe glacier from the NSIDC (National Snow and Ice Data Center; Fetterer and Windnagel2017). We show that although calving events occur in majority during periods of landfast sea-ice melting, the propagation of the fissure can take place in the middle of the austral winter when the ice tongue is totally embedded in sea-ice.

https://doi.org/10.5194/egusphere-2023-736
Preprint. Discussion started: 21 June 2023
© Author(s) 2023. CC BY 4.0 License.

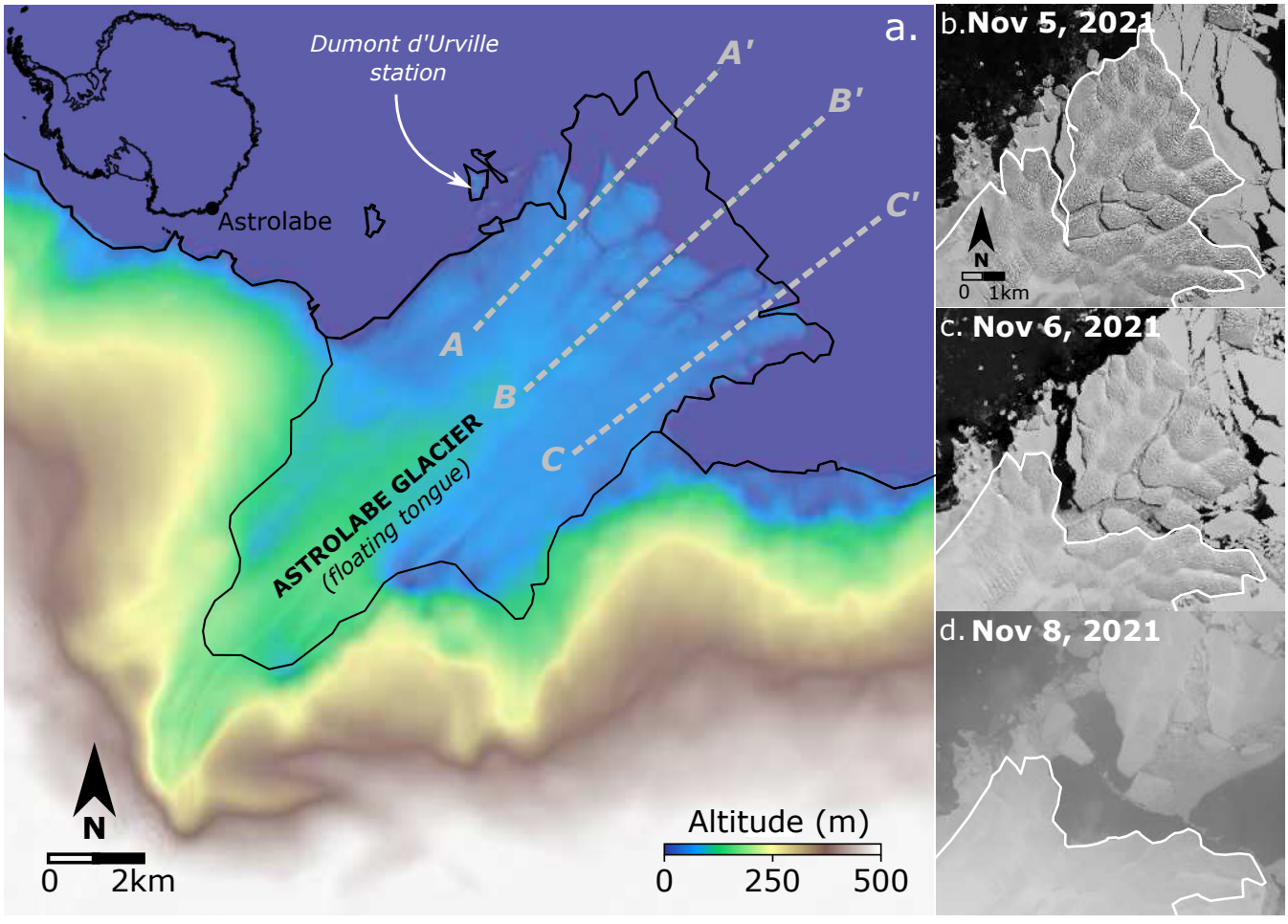

Figure 1. a) Map of the Astrolabe glacier with the coastline and grounding lines from (Gerrish, 2022) and the topography of the area (from the 2021 GLO30 Copernicus DEM at 30m resolution, https://doi.org/10.5270/ESA-c5d3d65) in the background. The location of the Astrolabe glacier is indicated in the small inset on the left upper corner. Figures b) to d) show the ice calving of November 2021 visible on b) Sentinel-2 acquisition of November 5, 2021, c) Landsat-8 acquisition of November 6, 2021 and d) November 8, 2021.

2 Data and methods

2.1 Satellite imagery

2.1.1 Mapping of the ice front position

55 The Ice front of the Astrolabe glacier was mapped using Landsat, ASTER and Sentinel-2 optical satellite images available in open access. The first satellite image available has been acquired by Landsat-4 on January 14, 1989 (Figure 1b). In total, 54 images are analyzed and the evolution of the ice front is mapped manually for four periods: 1989-1990 (Figure 1b), 2000-2010

https://doi.org/10.5194/egusphere-2023-736
Preprint. Discussion started: 21 June 2023
© Author(s) 2023. CC BY 4.0 License.

(Figure 1c), 2010-2020 (Figure 1d), and 2020-November 2021 (Figure 1e). No optical image is found for the period 1990-2000. The area of the floating tongue is estimated considering a reference grounding line position (Bindschadler et al. 2011; Figure 1a). A more precise delineation of the grounding line has been proposed by Le Meur et al., 2014.

2.1.2 Ice velocity monitoring from optical images

Satellite imagery is used to compute the ice velocity with image correlation techniques. (Avouac et al., 2006; Leprince et al., 2007; Rignot et al., 2011; Mouginot et al., 2017; Millan et al., 2022). These techniques consist in matching pixels from one image to another to retrieve the shift in the position of a particular feature through time. Several studies have shown the interest of this technique to monitor ice surface velocity (Dehecq et al., 2015; Altena et al., 2019) especially in polar regions (Joughin et al., 2018; Millan et al., 2022). We used the GDM-OPT-ICE service (Provost et al., 2022) to compute ice displacement time series. The GDM-OPT-ICE service allows for the precise co-registration of the satellite imagery stack using the CO-REGIS algorithm (Stumpf et al., 2018), computes the shift between pairs of co-registered images with the open source stereo-photogrammetric library MicMac (Rosu et al., 2015) and inverts the displacement time series with the TIO algorithm (Doin et al., 2011; Bontemps et al., 2018).

The Copernicus Sentinel-2 mission provides acquisitions over the Astrolabe glacier every three to six days, during the austral summer (September to April). In total, from February 2017 to early November 2021, 59 Sentinel-2 images were acquired with no overcast over the Astrolabe glacier. The pairing network is set up to pair each image successively with the five next acquisitions, resulting in 280 pairs. The correlation is computed on a window of 5 by 5 pixels using sub-pixel refinement. The displacement time series is inverted for each acquisition date with a spatial resolution of 1 by 1 pixel (i.e., 10 m x 10 m). The resulting displacement time series is interpolated at 30 days in order to compute the evolution of the ice velocity and reduce the noise.

2.1.3 Computation of the strain rates from the ice velocity fields

Strain is a measure of how much a medium (here ice) stretches, compresses and deforms in all directions as it flows, whereas strain rates represent how quickly these deformations occur. The strain rates can therefore be computed using satellite-derived velocity (Alley et al., 2018; Cheng et al., 2021). We used the method described in (Alley et al., 2018) and (Nye, 1959) to compute the longitudinal, transverse and shear strain rates using the yearly estimation of the ice velocity derived from the GDM-OPT-ICE outputs (see section 3.2.1). The strain rates are computed at a spatial resolution of 20 meters.

2.2 In situ sensors

2.2.1 On-site GNSS observations and displacement measurements

A permanent GNSS network (https://astrolabe.osug.fr/) is maintained by the Institut des Géosciences de l'Environnement (IGE) on the Astrolabe glacier. It consists of 8 GNSS stations in 2018 and 4 stations in 2021 (mainly because of a lack of maintenance in 2019/2020 due to cancellation of the summer operations in Antarctica because of the COVID pandemic). The

https://doi.org/10.5194/egusphere-2023-736
Preprint. Discussion started: 21 June 2023
© Author(s) 2023. CC BY 4.0 License.

GNSS receivers and antennas are mounted on beacons specifically designed for harsh environmental conditions (strong winds, local wind-drifted accumulation of snow, ice motion, summer melting leading to tilting or even collapse of the beacons). These harsh conditions explain some gaps in the GNSS time series, mainly during the austral winters. The receivers are geodetic dual-frequency receivers (Trimble™NetR9) connected to Zephir geodetic antennas. The GNSS observations consist of 3 two-hour measuring sessions per day where positions are averaged from 30-s sampling measurements. The positions are calculated for 24h measurements in PPP mode (Precise Point Positioning) using the GipsyX geodetic software (Zumberge et al., 1997). The accuracy is 1.5 cm (standard deviation 0.9 cm) in the horizontal component and 3.8 cm (standard deviation 2.7 cm) in the vertical component.

A field campaign was realized in 2020 to quantify the ice velocity in the vicinity of the grounding line position. It consists of 15 bamboo sticks that were implanted on the ice in January 2020 during one week. The position of the sticks was measured the first day and then, one week later, with a GNSS dual-frequency receiver, allowing for an estimation of the ice velocity.

3 Results

3.1 Ice front position: 2000-2021

Changes in the ice tongue surface Figure 2a-d, and ice front position along three profiles are presented in Figure 2e-g. Before 2007, the number of cloudless acquisitions per year is very limited (1-2 images). From 2006, Landsat-7 (and then Landsat-8 and Sentinel-2) provides 5 to more than 10 cloudless images per year, allowing to resolve the calving cycle of the Astrolabe glacier. Evolution of Profiles AA' (western profile) and BB' (central profile) exhibit a similar temporal evolution (Figure 2e, f). In particular, along those two profiles, the most advanced position of the ice tongue is 5 and 4 km for profile AA' and BB' respectively (Figure 2) with calving occurring regularly every 2 to 4 years. From 2016 to 2021, the ice tongue experienced a particularly long period of growth and reached an unprecedentedly observed position at 7.2 km and 6.7 km for profile AA' and BB' respectively. Conversely, the evolution of the ice front position on profile CC' remains from 2000 to 2021 at a maximum distance of 5.8 km (Figure 2g). Moreover, the occurrence of calving of this part of the ice tongue is significantly different from the central and western parts. Indeed, on profile CC', the ice front progresses regularly during 6 years from 2010 to 2016 when it regresses once in 2012 on profiles AA' and BB'. The ice tongue also experienced two calving events in the eastern side of the tongue in winter 2019-2020, and winter 2020-2021, while this is not observed on the other two profiles (Figure 2e-g). A linear regression is also performed to retrieve the velocity of the ice front progression in between the successive calving events (Figure 2e-g). The velocity varies highly from one period to another, but one can observe that the velocity are significantly lower for profile CC' (1.17 m.day^{-1}-1.55 m.day^{-1}) than for profile AA' (0.96 m.day^{-1}-1.79 m.day^{-1}) and BB' (1.75 m.day^{-1}-2.12 m.day^{-1}).

https://doi.org/10.5194/egusphere-2023-736
Preprint. Discussion started: 21 June 2023
© Author(s) 2023. CC BY 4.0 License.

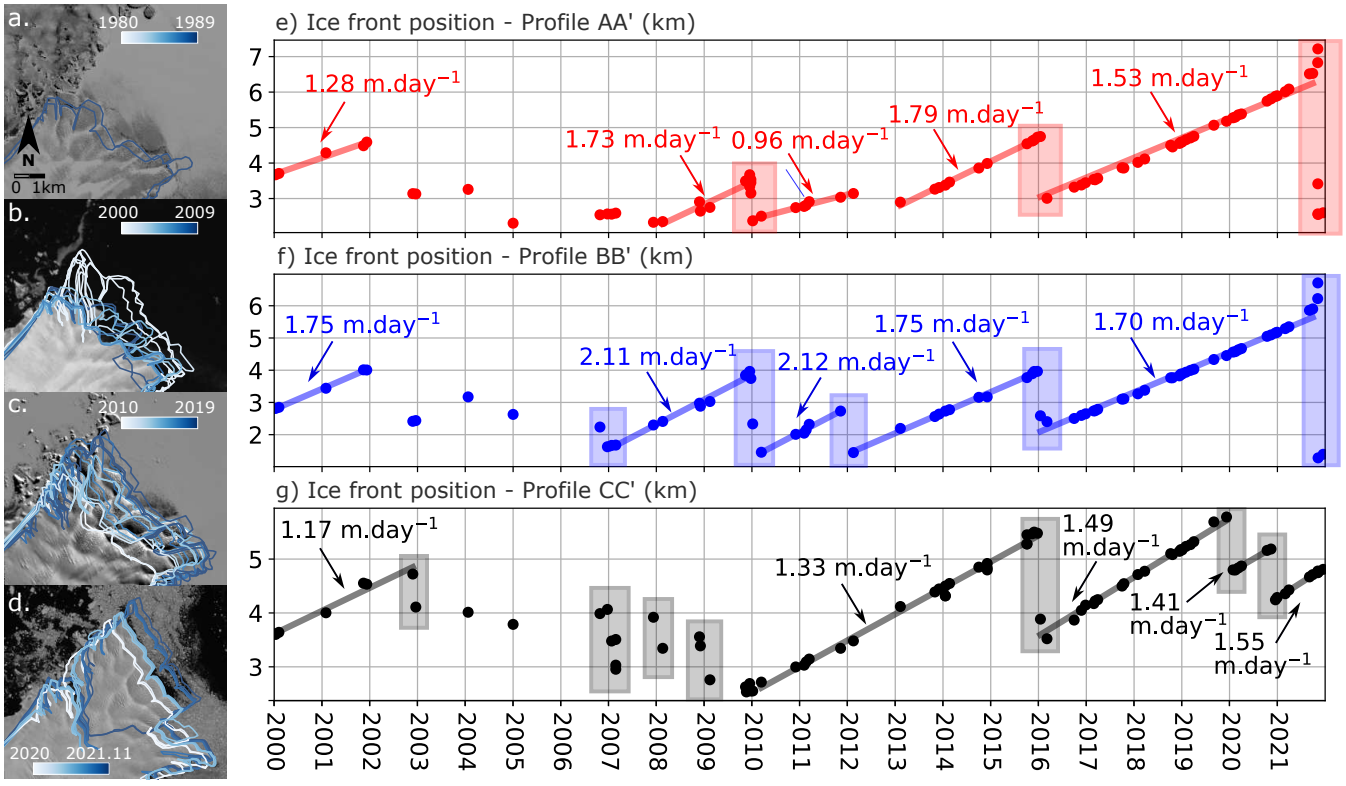

Figure 2. Evolution of the front position of the glacier for the periods a: 1980-1989, b: 2000-2010, c: 2010-2020 and d: January 2020 - November 2021. The background images are band-4 of Landsat-4, -7, -8 and Sentinel-2 chosen as representative of the period. Figures e-g present the position of the terminus of the glacier along profiles AA' (e), BB' (f) and CC'(g); see Figure 1a) for the location of the profiles). The velocity of the ice front motion is indicated for the periods of ice front progression and calving events are presented with boxes.

3.2 Ice velocity: 2017-2021

Ice velocity is plotted for each year from 2017 to 2021 (Figure 3a) together with the derived longitudinal, transversal and shear strain rates (Figure 3c, d, e respectively). Figure 3b presents the ice velocity computed with GDM-OPT-ICE and the velocity measured with in situ instrumentation (i.e., GNSS's and bambou sticks campaign). The yearly estimation obtained with GDM-OPT-ICE is compared to the one measured with in situ instrumentation. The velocity in this part of the glacier is very constant though time and do not exhibit seasonal variations. The comparison between the two datasets shows that the estimation of the velocity from GDM-OPT-ICE improves with time, with a poor accuracy in 2017 (RMS = 0.76 m.day^{-1}) and a much better one from 2019 (RMS $<$ 0.25 m.day^{-1}). One can observe that the gradient of velocity from the western border to the center of the glacier is well retrieved with the GDM-OPT-ICE products of 2019-2021 (Figure 3b). In 2017 and 2018, a large portion of the glacier is estimated to be stable from the results of the GDM-OPT-ICE whereas the GNSS's campaign of this year show

https://doi.org/10.5194/egusphere-2023-736
Preprint. Discussion started: 21 June 2023
© Author(s) 2023. CC BY 4.0 License.

that the position of the western glacier border is stable through time. The small number of cloudless Sentinel-2 acquisitions for those years may explain the low RMS error of these two years.

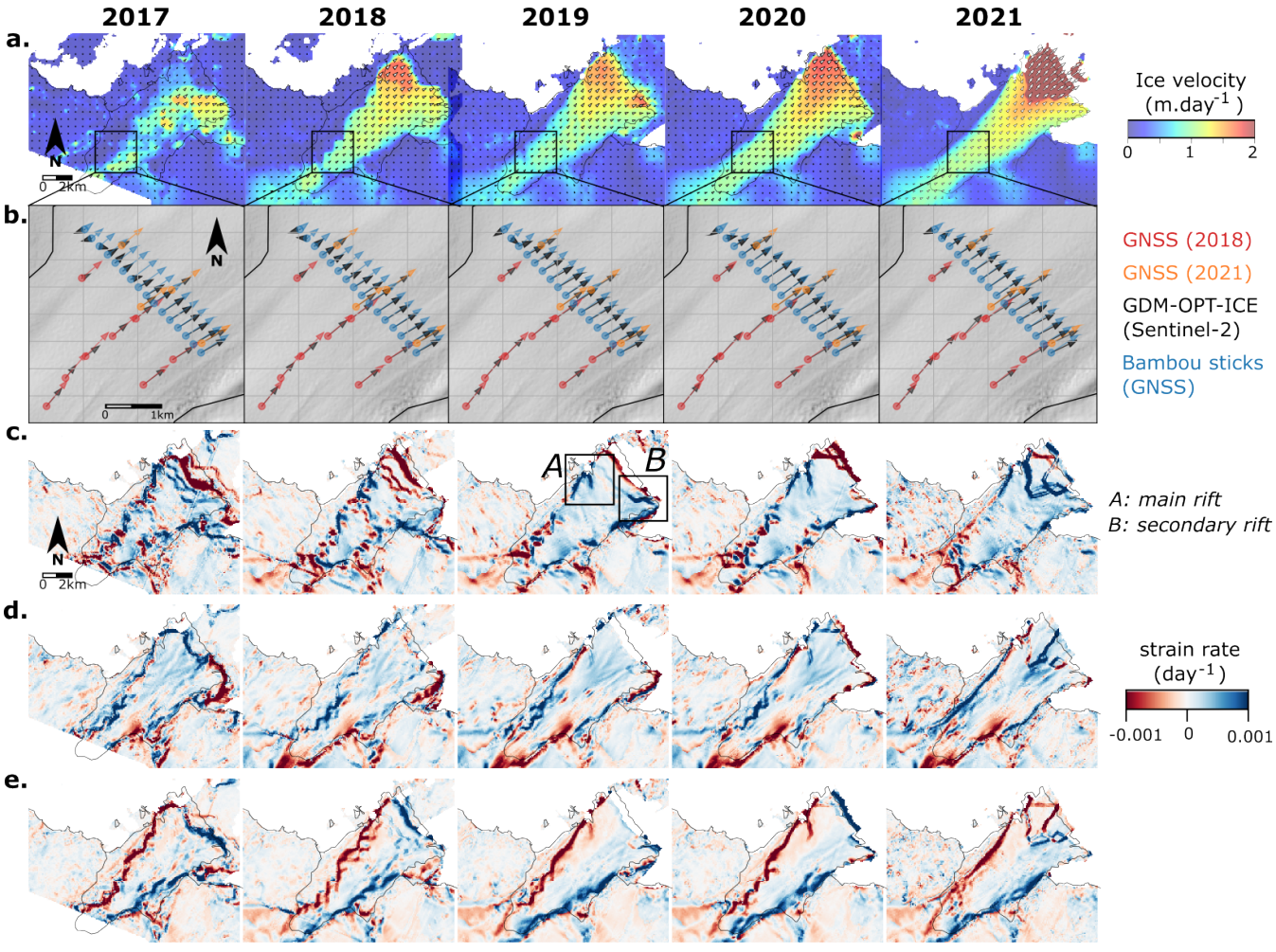

Figure 3. a) Yearly estimation of ice velocity for the Astrolabe glacier for the period 2017-2021, b) comparison of the velocity magnitude and direction as measured by the in situ instrumentation (GNSS's and bamboo sticks campaign) and as measured by GDM-OPT-ICE. Figures c, d, e present the longitudinal, transversal and shear strain rates derived from the ice velocity fields.

The velocity field shows a smooth gradient with lower velocity of circa 1 m.day^{-1} in the south-eastern part of the glacier and faster velocity of 1.2-1.5 m.day^{-1} in the north-western part of the glacier. In 2019, a small block of ice accelerated in the eastern part of the ice front (Figure 3a) also visible in the longitudinal strain rate field. This block disappears in both the mean velocity of 2020 (Figure 3a) and in the strain rate field (Figure 4c) and the calving of this part of the glacier occurred in December 2020 (Figure 2d, profile CC'). In 2019, an extensive fracture appeared in the longitudinal and shear components of the strain rate field in the western part of the ice tongue in front of the Dumont D'Urville station (Figure 4c, e). The northern-

https://doi.org/10.5194/egusphere-2023-736
Preprint. Discussion started: 21 June 2023
© Author(s) 2023. CC BY 4.0 License.

western part of the ice tongue starts simultaneously to exhibit larger velocities in 2020 and 2021 (Figure 3a). In 2021, a complex network of localized increase of strain rates appears on the western-northern part of the glacier delimiting the potential area of the future iceberg to be calved (Figure 3c, d, e). This complex network delimits the fractures that were observed on the ice in the first available summer acquisition in September 2021 and that remained the same until the ice calving (Figure 1f). Beside the evolution of the fractures on the ice, one can also observe the high strain rates (> 0.002 day^{-1}) that are clearly identifiable through time along the lateral limits of the glacier (Figure 3e).

3.3 Glacier acceleration and ice break off: 2021

The displacement time series is linearly interpolated over a time step of 30 days from the first acquisition in 2017 to November 5, 2021. Mean monthly velocity and strain rate fields are derived from this interpolation. We investigate the evolution of the strain rates for the period January and November 2021 to understand the dynamic of the recent calving (Figure 4). Strain rates maps show high concentration of strain localized along linear structures, which grow progressively from April 2021 to November 2021 (Figure 4a). These linear structures are not visible at the surface of the glacier (Figure 4c) until June 2021 except for the main rift in front of the Dumon D'Urville station. We set a threshold on the strain rates in order to analyze the evolution of these localized concentration of strain, as well as the occurrence of the spatial connection between them (Figure 4b). The evolution of their growth is complex, with transitions from one component to another. For example, the main rift exhibits a clear longitudinal strain rate from April 2021 to September 2021 that evolves toward a shear strain rate in October, November 2021 (Figure 4b). From May 2021, a large concentration of strain appears in the transverse component along another fracture oriented in the North-East/South-West direction (Figure 4a, b). Similarly, a third fracture appears in the longitudinal component on the eastern side (Figure 4a, b). These fractures grow rapidly and connect together in June 2021 (Figure 4b). We analyzed the Sentinel-1 SAR images from May 2021 to August 2021 in order to validate these observations. We observe that the network of fracture opened suddenly between June 13, 2021, and June 25, 2021 (Figure 4c, d) which is coherent with the timing of the connection derived from the time series of surface displacement. One can also observe that from October 2021, most of the fractures exhibit a shear strain rate, likely due to the rotation of the blocks. It can be noted that compressional strain rates are measured from 2017 to 2020 at the terminus of the glacier tongue with strain rate larger than 0.001 day^{-1} while it is not observed anymore in 2021 (Figure 3c).

3.4 Landfast sea-ice forcing

We analyze time series of sea-ice extent and concentration in the region of the Astrolabe glacier. The data for sea-ice extent and concentration were downloaded on the NSDIC repository (Fetterer and Windnagel, 2017). We cropped the data to analyze the monthly variation of the sea-ice extend over an area of 4000 km^2 around the Astrolabe glacier from 1979 to the end of 2021 (Figure 5a) and the daily variation of the sea ice concentration at the border of the Astrolabe glacier from 2000 to the end of 2021 (Figure 5b). We observe a significant change in the periodicity of sea-ice melt around the Astrolabe glacier in the last decade (2011-2021). Indeed, from 1979 to 2011, the extent of the sea-ice decreases significantly every year during the summer while from 2011 to 2021, two successive periods: 2012-2016 and 2016-2020, where the extent of the sea-ice remains maximal

https://doi.org/10.5194/egusphere-2023-736
Preprint. Discussion started: 21 June 2023
© Author(s) 2023. CC BY 4.0 License.

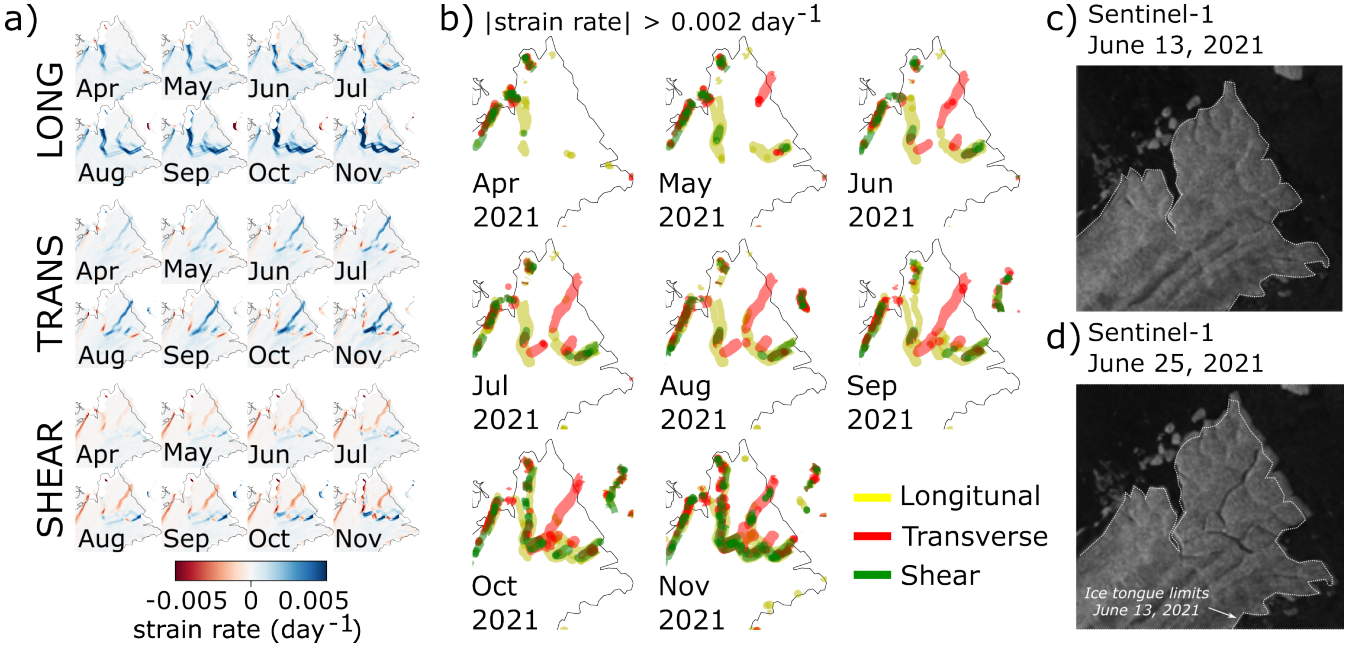

Figure 4. a) Monthly strain field derived from interpolated displacement time series, b) map of the strain rates larger than 0.002 day^{-1}. The three strain rate components (longitudinal, transverse and shear) are plotted together. Subsets c) and d) are showing the occurrence of the fractures detected with Sentinel-1 acquisitions of June 13 and June 25, 2021.

(Figure 5a). These periods of Multi-Year Fast sea-Ice (MYFI) are well correlated with periods of extension of the Astrolabe ice tongue (Figure 5a).

The time series of daily sea ice concentration shows similar observations. Before 2011, the sea ice concentration drop to 0% for periods of 2 to 3 months from November to mid-March with small variation on the length of sea-ice free periods. From 2008, the onset of the sea-ice free periods shifts from November to mid-December/January, while the end of the sea-ice free periods remain stable through time (Figure 5b). From 2012 to 2016, the sea ice free periods disappear or are shortened to one month and delayed to the month of February (Figure 5b). From 2017, the regime of sea ice concentration is highly variable, with years with no to very short periods of sea ice melt (2017, February 2020; Figure 5b) and years with prolonged sea ice melting (December 2018 - March 2019; November 2020 - March 2021). The date of the different calving events cannot be determined with daily precision, but one can observe that all calving occur when sea-ice concentration decreases to 0% at the end of the Austral fall (Figure 5b).

We also plot the evolution of the ice surface velocity along profile AA' and CC' from 2000 to November 2021 (Figure 5c, d). Yearly estimation of the velocity provided by the NASA MeaSUREs ITS_LIVE project (Gardner et al., 2018) are plotted for years 2000-2017. From 2017 onwards, the monthly velocity estimated from the GDM-OPT-ICE chain is plotted. Over the two last decades, we do not see significant variations in the ice velocity from 2000 to 2021 except for local accelerations (Figure 5c, d). We observe that the surface seems to flow slightly faster on the western part of the ice tongue (Profile AA', Figure 5c)

https://doi.org/10.5194/egusphere-2023-736
Preprint. Discussion started: 21 June 2023
© Author(s) 2023. CC BY 4.0 License.

than on the eastern part (Profile CC', Figure 5d) which is also observed in the velocity of the terminus position (Figure 2e-g). Local acceleration are visible in 2021 on profile AA' and in 2019 and 2020 for profile CC' (Figure **??**c, d) and correspond to the area of the glacier that calved in 2019, 2020 and 2021 (Figure **??**b). Before 2017, the yearly measures are cropped before the end of the ice tongue and the area where the fissures usually initiate is not mapped by the dataset. Moreover, the seasonal variations remain difficult to infer as optical data are not acquired during winter.

4 Discussion

The presence of rift and fracture networks in ice tongue several years to several months prior to calving has also been reported in other glaciers (Fricker et al., 2005; Walker et al., 2015; Cheng et al., 2021; Larour et al., 2021). However, we observe at the Astrolabe glacier's ice tongue that a complex network of fractures opened suddenly in the middle of June 2021 (Figure 4) at the tip, and in the transversal direction, of the pre-existing main rift that has grown regularly for 3 years (Figure 3). Few rift or fracture propagation are reported to occur during Austral winter (Walker et al., 2013; Larour et al., 2021). The critical thinning of the ice tongue due to its exceptional extension may explain this timing (Robel, 2017; Larour et al., 2021; Åström and Benn, 2019) although it would likely favor the propagation of the rift along the same direction as the pre-existing rift, which is not observed at the Astrolabe glacier (Figure 4). Instead, the main fracture propagating in June 2021 is oriented along the flow direction and opened in extension (Figure 4a, b). A possibility to explain the development of these fractures could be a transition from a ductile to a brittle behavior with the decrease of temperature during winter that may favor fractures along the flow resulting from the differential compressive load due to sea-ice buttressing and rift opening (Figure 4). This mechanism might be possible as the compressive longitudinal strain seems to disappear in 2021 at the glacier terminus (Figure 3c) and the rift opens progressively. However, such a scenario would maintain the ice tongue terminus at the same position due to the effect of sea-ice buttressing, which is not what is observed (Figure 4c, d). Moreover, the compressive strength of the ice is much higher than extensive strength (Benn et al., 2007). A possible mechanism could that the rupture results from extensive circumferential stress that appear when the unconfined part of the ice tongue reaches a certain extension (Wearing et al., 2020). Basal channels and basal melt may as well play a role in the dislocation of the ice tongue (Vaughan et al., 2012; Alley et al., 2023). The difference in the calving cycle and ice velocity between the eastern part and the western part of the glacier terminus also suggest that the bathymetry underneath the ice tongue controls the location and evolution of the rifts. Further modelling is necessary to understand the mechanisms that lead to the apparition of these fractures at this time of the year and with this geometry (Åström and Benn, 2019; Crawford et al., 2021; Alley et al., 2023).

To understand the recent evolution of the glacier, we investigated the evolution of landfast sea-ice in the vicinity of the ice tongue. Landfast sea-ice evolution is usually assumed to delay ice tongue break off and favor its extension by buttressing the ice tongues and protecting them from ocean swells (Massom et al., 2010, 2018; Rott et al., 2018; Gomez-Fell et al., 2022). We observed a significant change in the periodicity of landfast sea-ice in the recent decade (2011-2021) in comparison with the previous observations (1979-2011; Figure 5a). Indeed, in the period 2011-2021, multi-year landfast sea-ice occurred with no sea-ice melt, or very short and/or episodic periods of melting (Figure 5b) at the vicinity of the Astrolabe ice tongue. The recent

https://doi.org/10.5194/egusphere-2023-736
Preprint. Discussion started: 21 June 2023
© Author(s) 2023. CC BY 4.0 License.

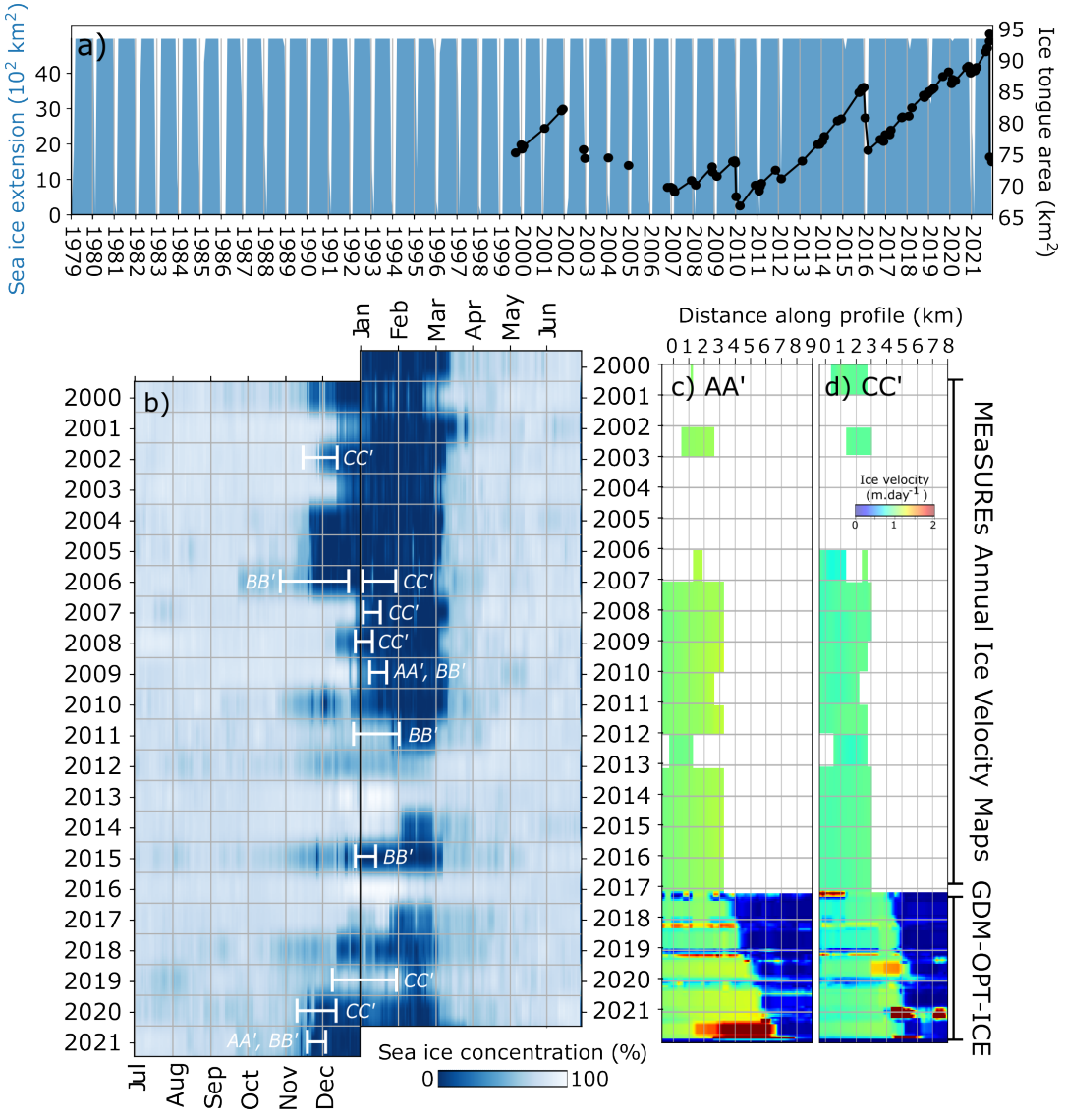

Figure 5. Evolution of monthly sea ice extent versus ice tongue extension (a), daily sea ice concentration (b) and ice tongue velocities along profile AA' (c) and CC' (d). Monthly sea ice extent is computed for a wide region of 4000 km^2 around the Astrolabe glacier (a) while the daily sea ice concentration is taken for the pixel of 25 km by 25 km at the Astrolabe ice tongue. Interval where observed calving have been observed are reported on the sub-figure (b) in white. The intervals usually span several days to weeks, depending on the availability of cloudless optical imagery. In years 2003-2005, calving likely occurred (see sub-figure a), although no observation can confirm the date. For the period 2000-2017, yearly estimation of the ice velocity from NASA MeaSUREs ITS_LIVE project (Gardner et al., 2018) are plotted while after 2017, monthly estimation of the velocity from the GDM-OPT-ICE processing chain are represented.

https://doi.org/10.5194/egusphere-2023-736
Preprint. Discussion started: 21 June 2023
© Author(s) 2023. CC BY 4.0 License.

periods of multi-year sea-ice presence are well correlated with the ice tongue spatial extension (Figure 5a) and seems to validate the assumption that sea-ice protect the ice tongue and favor its extension. We also observe that the calving systematically occur at the beginning of the sea-ice melting (Figure 5b) and is preceded by local accelerations of the areas that calved then (Figure 5c-d). These observations together with the presence of rifts visible several months/years before calving suggest that landfast sea-ice acts like a glue to hold together the ice tongue and have little effect to prevent rift opening at the Astrolabe ice tongue.

Landfast sea-ice is deeply connecting to regional and local atmospheric and oceanic states (Fogt et al., 2022). At the scale of the continent, records in Antarctica show a similar trend with a general positive increase of the sea ice extent from 1979 to 2016 with a minimum of global sea-ice extent recorded in summer 2017 (Fogt et al., 2022). In the region of the Astrolabe, Miles et al.2022 reports similar observations with the calving of the Commandant glacier in 2016 after multi-year expansion of this ice tongue between 2008 and 2016. These observations suggest that the calving of 2016 could be related to regional changes in the oceanic and atmospheric currents maybe similar to the ones observed in the Antarctica Peninsula (Christie et al., 2022). In 2021, the Astrolabe ice tongue reached an unprecedentedly observed advanced position with a total surface of 95 km^2. Due to the limited temporal extent of the datasets and sparse availability of the satellite imagery before the 2000s, it is impossible to conclude if these changes are exceptional or part of a longer cycle. However, the timing of the fracture suggests that the mechanisms that lead to the calving of November 2021 might have been different from the previous calving at the Astrolabe glacier. The recent increase in the frequency of satellite observations has significantly improved the glacier monitoring and recent calving (like the one of November 2021 at the Astrolabe) could be documented almost day by day with open access optical satellite imagery (Figure 1f, g, h) while before 2010, 1 to 2 images per year at most are available during summer. The dataset gathered in this study could be completed with the processing of radar imagery to monitor the glacier seasonal velocity variations and document more precisely the evolution of the rift propagation during winter, where optical acquisitions are not available. Radar interformetry (InSAR) could also be used to map the evolution of the glacier elevation and the position of the grounding line.

5 Conclusions

In this study, we analyzed the evolution of the Astrolabe glacier located in Terre Adélie, Antarctica. We used open access optical satellite imagery (ASTER, Landsat and Sentinel-2) to map the evolution of the ice front from 2000 to 2022. We also measure the surface velocity and derived strain rate fields between 2017 and 2022, using image correlation of Sentinel-2 images. The recent evolution of the glacier shows an unprecedentedly documented extension of 95 km^2 favored by the concomitant high concentration of the landfast sea ice in the region of Antarctica during 2011-2021 in comparison with previous records (2000-2011). The early melt of the sea ice in November 2021 favored the released of a 20 km^2 iceberg in the north-western part of the Astrolabe glacier. This is the first time a calving of this magnitude is documented at the Astrolabe glacier. We also observed that a complex network of fractures opened during the austral winter in June 2021 several months before the iceberg calving. This study shows the importance of ice velocity and strain rates fields time series derived from optical satellite imagery at high resolution to document fracture opening and raises further questions on the mechanism of rift propagation.

https://doi.org/10.5194/egusphere-2023-736
Preprint. Discussion started: 21 June 2023
© Author(s) 2023. CC BY 4.0 License.

Data availability. We acknowledge the use of imagery from Copernicus Sentinel-1 and 2 data and NASA ASTER and Landsat images (through https://earthexplorer.usgs.gov/). The GNSS observations are accessible on the Astrolabe repository: https://astrolabe.osug.fr/.

Author contributions. FP designed the experiments with contributions from DZ, ELM, JPM and CH. ELM provided the GNSS data and JPM processed them. FP processed the satellite data. All co-authors participated in the writing and/or revision and approval of the submitted manuscript

Competing interests. We have no competing interests.

Acknowledgements. The GDM-OPT-ICE service is developed and maintained by ForM@Ter (Data and Service for the Solid Earth: en.poleterresolide.fr) and exploited on the EOST/A2S High Performance Computing (HPC) infrastructure of University of Strasbourg (1.5 Tier Mesocentre) allowing optimized computation. The service is accessible on-demand through the ForM@Ter data hub (en.poleterresolide.fr/services-en/gdm-en/#/optic) and the Geohazards Exploitation Platform (GEP: geohazards-tep.eu). The authors also acknowledge the support of the French Agence Nationale de la Recherche (ANR), under grant ANR-20-CE01-0006 (project HighLand).

https://doi.org/10.5194/egusphere-2023-736
Preprint. Discussion started: 21 June 2023
© Author(s) 2023. CC BY 4.0 License.

References

Alley, K. E., Scambos, T. A., Anderson, R. S., Rajaram, H., Pope, A., and Haran, T. M.: Continent-wide estimates of Antarctic strain rates from Landsat 8-derived velocity grids, Journal of Glaciology, 64, 321–332, 2018.

Alley, K. E., Scambos, T. A., and Alley, R. B.: The role of channelized basal melt in ice-shelf stability: recent progress and future priorities, Annals of Glaciology, p. 1–5, https://doi.org/10.1017/aog.2023.5, 2023.

Altena, B., Haga, O. N., Nuth, C., and Kääb, A.: Monitoring Sub-Weekly Evolution of Surface Velocity and Elevation for a High-Latitude Surging Glacier using Sentinel-2, ISPRS - International Archives of the Photogrammetry, Remote Sensing and Spatial Information Sciences, XLII-2/W13, 1723–1727, https://doi.org/10.5194/isprs-archives-XLII-2-W13-1723-2019, 2019.

Åström, J. A. and Benn, D. I.: Effective rheology across the fragmentation transition for sea ice and ice shelves, Geophysical Research Letters, 46, 13 099–13 106, 2019.

Avouac, J.-P., Ayoub, F., Leprince, S., Konca, O., and Helmberger, D. V.: The 2005, Mw 7.6 Kashmir earthquake: Sub-pixel correlation of ASTER images and seismic waveforms analysis, Earth and Planetary Science Letters, 249, 514–528, 2006.

Banwell, A. F., MacAyeal, D. R., and Sergienko, O. V.: Breakup of the Larsen B Ice Shelf triggered by chain reaction drainage of supraglacial lakes, Geophysical Research Letters, 40, 5872–5876, 2013.

Benn, D. I., Warren, C. R., and Mottram, R. H.: Calving processes and the dynamics of calving glaciers, Earth-Science Reviews, 82, 143–179, 2007.

Bindschadler, R., Choi, H., Wichlacz, A., Bingham, R., Bohlander, J., Brunt, K., Corr, H., Drews, R., Fricker, H., Hall, M., et al.: Getting around Antarctica: new high-resolution mappings of the grounded and freely-floating boundaries of the Antarctic ice sheet created for the International Polar Year, The Cryosphere, 5, 569–588, 2011.

Bontemps, N., Lacroix, P., and Doin, M.-P.: Inversion of deformation fields time-series from optical images, and application to the long term kinematics of slow-moving landslides in Peru, Remote Sensing of Environment, 210, 144 – 158, https://doi.org/https://doi.org/10.1016/j.rse.2018.02.023, 2018.

Borstad, C., McGrath, D., and Pope, A.: Fracture propagation and stability of ice shelves governed by ice shelf heterogeneity, Geophysical Research Letters, 44, 4186–4194, 2017.

Chambers, C., Greve, R., Obase, T., Saito, F., and Abe-Ouchi, A.: Mass loss of the Antarctic ice sheet until the year 3000 under a sustained late-21st-century climate, Journal of Glaciology, 68, 605–617, 2022.

Cheng, Y., Xia, M., Qiao, G., Lv, D., Li, Y., and Hai, G.: Imminent calving accelerated by increased instability of the Brunt Ice Shelf, in response to climate warming, Earth and Planetary Science Letters, 572, 117 132, 2021.

Christie, F. D., Benham, T. J., Batchelor, C. L., Rack, W., Montelli, A., and Dowdeswell, J. A.: Antarctic ice-shelf advance driven by anomalous atmospheric and sea-ice circulation, Nature Geoscience, 15, 356–362, 2022.

Crawford, A. J., Benn, D. I., Todd, J., Åström, J. A., Bassis, J. N., and Zwinger, T.: Marine ice-cliff instability modeling shows mixed-mode ice-cliff failure and yields calving rate parameterization, Nature communications, 12, 2701, 2021.

Dehecq, A., Gourmelen, N., and Trouve, E.: Deriving large-scale glacier velocities from a complete satellite archive: Application to the Pamir–Karakoram–Himalaya, Remote Sensing of Environment, 162, 55 – 66, https://doi.org/https://doi.org/10.1016/j.rse.2015.01.031, 2015.

https://doi.org/10.5194/egusphere-2023-736
Preprint. Discussion started: 21 June 2023
© Author(s) 2023. CC BY 4.0 License.

Doin, M.-P., Guillaso, S., Jolivet, R., Lasserre, C., Lodge, F., Ducret, G., and Grandin, R.: Presentation of the small baseline NSBAS processing chain on a case example: the Etna deformation monitoring from 2003 to 2010 using Envisat data, in: Proceedings of the Fringe symposium, pp. 3434–3437, ESA SP-697, Frascati, Italy, 2011.

Fetterer, F., K. K. W. N. M. M. S. and Windnagel, A. K.: Sea Ice Index, Version 3, https://doi.org/10.7265/N5K072F8, 2017.

Fogt, R. L., Sleinkofer, A. M., Raphael, M. N., and Handcock, M. S.: A regime shift in seasonal total Antarctic sea ice extent in the twentieth century, Nature Climate Change, 12, 54–62, 2022.

Fricker, H., Young, N., Coleman, R., Bassis, J., and Minster, J.-B.: Multi-year monitoring of rift propagation on the Amery Ice Shelf, East Antarctica, Geophysical Research Letters, 32, 2005.

Gardner, A. S., Moholdt, G., Scambos, T., Fahnstock, M., Ligtenberg, S., Van Den Broeke, M., and Nilsson, J.: Increased West Antarctic and unchanged East Antarctic ice discharge over the last 7 years, The Cryosphere, 12, 521–547, 2018.

Gerrish, L., F. P. . C. P.: High resolution vector polylines of the Antarctic coastline (7.6) [Data set], https://doi.org/https://doi.org/10.5285/45174e8c-7ce8-4d87-a6f7-570db476c6c9, 2022.

Gomez-Fell, R., Rack, W., Purdie, H., and Marsh, O.: Parker Ice Tongue Collapse, Antarctica, Triggered by Loss of Stabilizing Land-Fast Sea Ice, Geophysical Research Letters, 49, e2021GL096 156, 2022.

Gudmundsson, G. H., Paolo, F. S., Adusumilli, S., and Fricker, H. A.: Instantaneous Antarctic ice sheet mass loss driven by thinning ice shelves, Geophysical Research Letters, 46, 13 903–13 909, 2019.

Joughin, I., Smith, B. E., and Howat, I. M.: A complete map of Greenland ice velocity derived from satellite data collected over 20 years, Journal of Glaciology, 64, 1–11, 2018.

Larour, E., Rignot, E., Poinelli, M., and Scheuchl, B.: Physical processes controlling the rifting of Larsen C Ice Shelf, Antarctica, prior to the calving of iceberg A68, Proceedings of the National Academy of Sciences, 118, 2021.

Le Meur, E., Sacchettini, M., Garambois, S., Berthier, E., Drouet, A., Durand, G., Young, D., Greenbaum, J., Holt, J., Blankenship, D., et al.: Two independent methods for mapping the grounding line of an outlet glacier–an example from the Astrolabe Glacier, Terre Adélie, Antarctica, The Cryosphere, 8, 1331–1346, 2014.

Leprince, S., Barbot, S., Ayoub, F., and Avouac, J.-P.: Automatic and precise orthorectification, coregistration, and subpixel correlation of satellite images, application to ground deformation measurements, IEEE Transactions on Geoscience and Remote Sensing, 45, 1529–1558, 2007.

Liu, Y., Moore, J. C., Cheng, X., Gladstone, R. M., Bassis, J. N., Liu, H., Wen, J., and Hui, F.: Ocean-driven thinning enhances iceberg calving and retreat of Antarctic ice shelves, Proceedings of the National Academy of Sciences, 112, 3263–3268, 2015.

Massom, R., Hill, K., Lytle, V., Worby, A., Paget, M., and Allison, I.: Effects of regional fast-ice and iceberg distributions on the behaviour of the Mertz Glacier polynya, East Antarctica, Annals of Glaciology, 33, 391–398, 2001.

Massom, R., Giles, A. B., Fricker, H. A., Warner, R. C., Legrésy, B., Hyland, G., Young, N., and Fraser, A. D.: Examining the interaction between multi-year landfast sea ice and the Mertz Glacier Tongue, East Antarctica: Another factor in ice sheet stability?, Journal of Geophysical Research: Oceans, 115, 2010.

Massom, R., Scambos, T. A., Bennetts, L. G., Reid, P., Squire, V. A., and Stammerjohn, S. E.: Antarctic ice shelf disintegration triggered by sea ice loss and ocean swell, Nature, 558, 383–389, 2018.

Miles, B. W., Stokes, C. R., and Jamieson, S. S.: Simultaneous disintegration of outlet glaciers in Porpoise Bay (Wilkes Land), East Antarctica, driven by sea ice break-up, The Cryosphere, 11, 427–442, 2017.

https://doi.org/10.5194/egusphere-2023-736
Preprint. Discussion started: 21 June 2023
© Author(s) 2023. CC BY 4.0 License.

Miles, B. W., Stokes, C. R., Jamieson, S. S., Jordan, J. R., Gudmundsson, G. H., and Jenkins, A.: High spatial and temporal variability in Antarctic ice discharge linked to ice shelf buttressing and bed geometry, Scientific reports, 12, 1–14, 2022.

Millan, R., Mouginot, J., Rabatel, A., and Morlighem, M.: Ice velocity and thickness of the world's glaciers, Nature Geoscience, 15, 124–129, 2022.

Mouginot, J., Rignot, E., Scheuchl, B., and Millan, R.: Comprehensive annual ice sheet velocity mapping using Landsat-8, Sentinel-1, and RADARSAT-2 data, Remote Sensing, 9, 364, 2017.

Nye, J. F.: A method of determining the strain-rate tensor at the surface of a glacier, Journal of Glaciology, 3, 409–419, 1959.

Olinger, S., Lipovsky, B., Wiens, D., Aster, R., Bromirski, P., Chen, Z., Gerstoft, P., Nyblade, A., and Stephen, R.: Tidal and thermal stresses drive seismicity along a major Ross Ice Shelf rift, Geophysical Research Letters, 46, 6644–6652, 2019.

Paolo, F. S., Fricker, H. A., and Padman, L.: Volume loss from Antarctic ice shelves is accelerating, Science, 348, 327–331, 2015.

Pritchard, H., Ligtenberg, S. R., Fricker, H. A., Vaughan, D. G., van den Broeke, M. R., and Padman, L.: Antarctic ice-sheet loss driven by basal melting of ice shelves, Nature, 484, 502–505, 2012.

Provost, F., Michéa, D., Malet, J.-P., Boissier, E., Pointal, E., Stumpf, A., Pacini, F., Doin, M.-P., Lacroix, P., Proy, C., and Bally, P.: Terrain deformation measurements from optical satellite imagery: The MPIC-OPT processing services for geohazards monitoring, Remote Sensing of Environment, 274, 112 949, 2022.

Rignot, E., Mouginot, J., and Scheuchl, B.: Ice flow of the Antarctic ice sheet, Science, 333, 1427–1430, 2011.

Rignot, E., Mouginot, J., Scheuchl, B., Van Den Broeke, M., Van Wessem, M. J., and Morlighem, M.: Four decades of Antarctic Ice Sheet mass balance from 1979–2017, Proceedings of the National Academy of Sciences, 116, 1095–1103, 2019.

Ritz, C., Edwards, T. L., Durand, G., Payne, A. J., Peyaud, V., and Hindmarsh, R. C.: Potential sea-level rise from Antarctic ice-sheet instability constrained by observations, Nature, 528, 115–118, 2015.

Robel, A. A.: Thinning sea ice weakens buttressing force of iceberg mélange and promotes calving, Nature Communications, 8, 1–7, 2017.

Rosu, A.-M., Pierrot-Deseilligny, M., Delorme, A., Binet, R., and Klinger, Y.: Measurement of ground displacement from optical satellite image correlation using the free open-source software MicMac, ISPRS Journal of Photogrammetry and Remote Sensing, 100, 48 – 59, https://doi.org/https://doi.org/10.1016/j.isprsjprs.2014.03.002, high-Resolution Earth Imaging for Geospatial Information, 2015.

Rott, H., Abdel Jaber, W., Wuite, J., Scheiblauer, S., Floricioiu, D., Van Wessem, J. M., Nagler, T., Miranda, N., and Van Den Broeke, M. R.: Changing pattern of ice flow and mass balance for glaciers discharging into the Larsen A and B embayments, Antarctic Peninsula, 2011 to 2016, The Cryosphere, 12, 1273–1291, 2018.

Scambos, T. A., Hulbe, C., Fahnestock, M., and Bohlander, J.: The link between climate warming and break-up of ice shelves in the Antarctic Peninsula, Journal of Glaciology, 46, 516–530, 2000.

Seroussi, H., Nowicki, S., Payne, A. J., Goelzer, H., Lipscomb, W. H., Abe-Ouchi, A., Agosta, C., Albrecht, T., Asay-Davis, X., Barthel, A., et al.: ISMIP6 Antarctica: a multi-model ensemble of the Antarctic ice sheet evolution over the 21st century, The Cryosphere, 14, 3033–3070, 2020.

Stumpf, A., Michéa, D., and Malet, J.-P.: Improved Co-Registration of Sentinel-2 and Landsat-8 Imagery for Earth Surface Motion Measurements, Remote Sensing, 10, 160, https://doi.org/10.3390/rs10020160, 2018.

Vaughan, D. G., Corr, H. F., Bindschadler, R. A., Dutrieux, P., Gudmundsson, G. H., Jenkins, A., Newman, T., Vornberger, P., and Wingham, D. J.: Subglacial melt channels and fracture in the floating part of Pine Island Glacier, Antarctica, Journal of Geophysical Research: Earth Surface, 117, 2012.

https://doi.org/10.5194/egusphere-2023-736
Preprint. Discussion started: 21 June 2023
© Author(s) 2023. CC BY 4.0 License.

Walker, C. C., Bassis, J., Fricker, H., and Czerwinski, R.: Structural and environmental controls on Antarctic ice shelf rift propagation inferred from satellite monitoring, Journal of Geophysical Research: Earth Surface, 118, 2354–2364, 2013.

Walker, C. C., Bassis, J. N., Fricker, H. A., and Czerwinski, R. J.: Observations of interannual and spatial variability in rift propagation in the Amery Ice Shelf, Antarctica, 2002–14, Journal of Glaciology, 61, 243–252, 2015.

Wearing, M. G., Kingslake, J., and Worster, M. G.: Can unconfined ice shelves provide buttressing via hoop stresses?, Journal of Glaciology, 66, 349–361, 2020.

Zumberge, J. F., Heflin, M. B., Jefferson, D. C., Watkins, M. M., and Webb, F. H.: Precise point positioning for the efficient and robust analysis of GPS data from large networks, Journal of Geophysical Research: Solid Earth, 102, 5005–5017, https://doi.org/https://doi.org/10.1029/96JB03860, 1997.